Novel Sensor Clustering–Based Approach for Simultaneous Detection of Stiffness and Mass Changes Using Output-Only Data

Article *in* Journal of Structural Engineering · July 2014

DOI: 10.1061/(ASCE)ST.1943-541X.0001218

A Novel Sensor Clustering-Based Approach for Simultaneous Detection of Stiffness and Mass Changes Using Output-only Data

[1]Qipei Mei and [2]Mustafa Gül

[1]Graduate Student

[2]Assistant Professor (Corresponding Author: mustafa.gul@ualberta.ca)

Department of Civil and Environmental Engineering, University of Alberta

Edmonton, Alberta, T6G 2W2, Canada

Abstract

This paper presents a novel sensor clustering-based time series approach for anomaly detection. The basic idea of this approach is that localized change in the properties of a structure may affect the relationship between the accelerations around the position where the damage occurs. Therefore, for both healthy and damaged (or unknown state) structures, Auto-Regressive Moving Average Models with eXogenous inputs (ARMAX) are created for different clusters using the data from the sensors in these clusters. The difference of the ARMAX model coefficients are employed as damage features (DFs) to determine the existence, location and severity of the damage. In order to verify this approach, it is first applied to a 4-DOF mass spring system and then to the shear type IASC-ASCE numerical benchmark problem. It is shown that the approach performs successfully for different damage patterns. It is also demonstrated that the approach can not only accurately determine the location and severity of the damage, but can also distinguish between changes in stiffness and mass.

1 *Introduction*

As infrastructure systems age and deteriorate, the focus of civil engineers and researchers gradually shifts from the design of structures to the maintenance of structures. The importance of developing robust automated systems that can detect anomalies in structures caused by either deterioration or extreme loading has been widely recognized in recent decades (Bernal and Beck 2004; Fan and Qiao 2011; Inaudi and Glisic 2008; Lynch and Loh 2006). In this context, Structural Health Monitoring (SHM) is acknowledged as an invaluable tool to assess the condition of critical infrastructures. In the last couple decades, owing mostly to the rapid progress of modern technologies, especially in the areas of computer science and electrical engineering, data acquisition has become much easier than ever before. Due to wider availability of the related technologies, various SHM techniques have been applied in different contexts (Pandey et al. 1991; Hearn and Testa 1991; Hou et al. 2000; Im et al. 2011; Moaveni et al. 2012; Han et al. 2014; Dharap et al. 2006). In particular, a number of long-term monitoring systems have been installed on bridges and buildings.

In general, SHM methods can be classified into two types, local methods and global methods (Johnson et al. 2004). Local methods aim to detect the damage in a localized region at a particular time using various techniques such as ultrasonics and x-ray (Kessler et al. 2002; Hola and Schabowicz 2010; Cheng and Tian 2012). Global methods, also widely known as vibration-based methods, assess the condition of the entire structure using the dynamic response of the structure. Vibration-based methods are economical and effective in assessing the overall health of the

structure, although some issues, such as the following, must be resolved before they are applied in reality (Beck and Bernal 2001): (1) modal characteristics are generally very insensitive to localized damage and damage may not be detected by damage features extracted from modal frequencies or mode shapes; (2) input force usually excites only the lower modes; (in many cases, such as ambient vibrations, the input signals cannot even be recorded); (3) the dynamic response data are available only at certain positions due to the limited number of sensors; and (4) an inverse problem needs to be resolved since the change of dynamic responses does not directly show what physical parameters have changed.

To overcome these issues, a number of parametric or non-parametric methods based on vibration data have been proposed (Gül and Catbas 2009; Nigro et al. 2014; Meruane and Heylen 2011; Ji et al. 2010). Parametric techniques aim to develop physics-based models for damage detection, most of which need to interact with finite element models (Shiradhonkar and Shrikhande 2011; Jafarkhani and Masri 2011; Moaveni 2009, Sipple and Sanayei 2013). Although these approaches are very effective in establishing a direct relationship between the DFs and the physical characteristics of the structure, developing the necessary models and analyzing the data may require significant experience, and for some cases the model may not even be identified correctly using limited data (Catbas et al. 2007). Given these factors, non-parametric methods using algorithms such as neural networks and time series analysis have recently attracted significant attention (Chang et al. 2000; Sohn et al. 2001, Taha 2010; Carden and Brownjohn 2008).

In this paper, a non-parametric method using time series analysis is introduced for damage detection. A time series is a sequence of data with uniform time intervals. Typical time series includes population, stock price, and temperature. Time series analyses are in general used to analyze time series data in order to extract the statistical characteristics of the data sets. Common time series models include Auto-Regressive (AR) models, Moving Average (MA) models, and Box-Jenkins (B-J) models. Early in their development, these methods had been mainly used in economics and electrical engineering. In 2001, Sohn et al. (2001) demonstrated a time series approach to detect damage. They combined Auto-Regressive models (AR models) with Auto-Regressive models with exogenous inputs (ARX models), and defined the residual error as the DF to detect damage. Subsequently, time series analysis garnered significant attention from researchers in the SHM area due to its potential for automated analysis.

More recently, significant effort has been spent developing the capability to detect, locate, and quantify damage. Monroig and Fujino (2006) derived an approach using second-order ARX models based on the equation of motion of a structure. They applied their approach to a structure similar to the ASCE benchmark problem in Bernal and Beck (2004). The results of their study were promising, showing that damage can be identified and located, although there were some false-positive and false-negative results. Gül and Catbas (2009) tested a statistical pattern recognition methodology in the context of time series analysis using different laboratory structures, showing that this methodology works well in most cases. However, they also identified some issues that would have to be resolved before applying this approach in a realistic structure, such as the determination of the

threshold. Figueiredo et al. (2012) applied time series models to data obtained using a piezoelectric active-sensing technique and extracted DFs as parameters of the models. Correlation analysis and principle component analysis were then used to determine the damage state, and a machine learning algorithm was adopted to remove the effect of environmental variability. The experimental results from a composite plate demonstrated that damage can be correctly identified.

1.1 *Objective and Scope*

As summarized above, time series modeling has great potential as a tool for damage detection. However, there are still a number of issues that must be addressed before it can be effectively used in real-life structures. In this paper, a novel damage detection method applying an Auto-Regressive Moving Average model with eXogenous inputs (ARMAX model) is presented. Developed based on previous work conducted by the authors (Gül and Catbas 2011; Mei and Gül 2013), the novelty of this approach compared to other approaches is that it can identify changes in the stiffness and mass of the system separately using the output-only data. The proposed method can accurately identify, locate, and quantify changes to these physical parameters in the numerical case studies with artificial noise investigated, enabling estimation of the location and extent of the damage. The following sections discuss the theoretical basis of the proposed methodology, along with results from the case studies. Current limitations of the methodology, such as being applicable only to shear-type structures in the current form, are also discussed.

2 *Outline of damage detection method and underlying theory*

2.1 *Time series modeling*

The time series model used in this paper is the ARMAX model. A brief introduction to this model is given below. Further details about this model can be found in the literature (Box et al. 2013; Brockwell and Davis 2002). The basic form of the ARMAX process with no delay term is given in Eq. (1),

$$\begin{aligned} y(t)+a_1y(t-\Delta t)+\mathrm{L}\ +a_{n_a}y(t-n_a\Delta t)=b_1u(t-\Delta t)+b_2u(t-2\Delta t)+\mathrm{L}\ +b_{n_b}u(t-n_b\Delta t) \\ +e(t)+d_1e(t-\Delta t)+\mathrm{L}\ +d_{n_c}e(t-n_c\Delta t) \end{aligned} \tag{1}$$

where $y(t)$ is the output, $u(t)$ is the input of the model, $e(t)$ is the error term, and $a_1,\mathrm{L}\ a_{n_a},b_1,\mathrm{L}\ b_{n_b},d_1,\mathrm{L}\ d_{n_c}$ are the parameters of the model. It is usually convenient to use the more concise form in Eq. (2),

$$A(q)y(t)=B(q)u(t)+D(q)e(t) \tag{2}$$

in which q is a back shift operator, meaning that a variable, say $X(t)$, at time t multiplied by q^j is equal to $X(t\text{-}j\Delta t)$. Therefore, the coefficients $A(q)$, $B(q)$, and $D(q)$ can be expressed in Eq. (3) by comparing Eq. (1) and Eq. (2); n_a, n_b and n_c are referred to as the orders of the parameters. ARMAX modeling is a more general form of AR modeling and Moving Average (MA) modeling. The time series $y(t)$ is called an AR process with order n_a if n_b and n_c are both zero, and an MA process with order n_c if n_a and n_b are zero. The exogenous inputs in ARMAX refers to $u(t)$ in Eq. (2), which is a different sequence than $y(t)$.

$$
\begin{aligned}
A(q) &= 1 + a_1 q^{-1} + \mathrm{L} \; + a_{n_a} q^{-n_a} \\
B(q) &= b_1 q^{-1} + b_2 q^{-2} \mathrm{L} \; + b_{n_b} q^{-n_b} \\
D(q) &= 1 + d_1 q^{-1} + \mathrm{L} \; + d_{n_c} q^{-n_c}
\end{aligned} \tag{3}
$$

2.2 *Creating the ARMAX models for different sensor clusters*

Shown in Eq. (4) is the equation of motion for an *N* degrees of freedom (DOF) linear dynamic system (time, *t*, has been omitted), which reveals the relationship between the dynamic response and excitation, where ***M***, ***C***, and ***K*** represent the mass, damping, and stiffness properties of the system, respectively. The vectors $\ddot{\boldsymbol{x}}$, $\dot{\boldsymbol{x}}$, and $\boldsymbol{x}$ correspond to accelerations, velocities, and displacements, respectively. The external forcing functions on the system are denoted by ***f***.

$$
\boldsymbol{M}\ddot{\boldsymbol{x}}(t) + \boldsymbol{C}\dot{\boldsymbol{x}}(t) + \boldsymbol{K}\boldsymbol{x}(t) = \boldsymbol{f}(t) \tag{4}
$$

In order to fit the dynamic responses of the system to ARMAX models in the context of the proposed methodology, some transformations must be conducted. First, the i^{th} row of Eq. (4) is considered separately as in Eq. (5). Re-arranging Eq. (5), Eq. (6) is obtained to represent the acceleration term of the i^{th} channel in terms of the other terms. Assuming that the structure has a lumped mass matrix, the acceleration terms on the right side are removed, since any off-diagonal entries of the mass matrix are zero. In addition, according to our investigation, the damping terms make very little contribution to the balance of the equation. Therefore, we neglect the damping terms as in Eq. (7). Considering that it is usually not practical to measure the displacement data in real-life applications, efforts are made to eliminate these terms from Eq. (7). By taking the second derivative of Eq. (7), we obtain the fourth derivative of *x* on the left side and accelerations on the

right side as in Eq. (8). Eq. (9) can then be obtained by applying the forward difference method (Levy and Lessman 1992) twice to Eq. (8); (the symbol, *t*, is added in these equations for further clarity).

$$\left(m_{i1}\ddot{x}_1+\mathrm{L}\ +m_{iN}\ddot{x}_N\right)+\left(c_{i1}\dot{x}_1+\mathrm{L}\ +c_{iN}\dot{x}_N\right)+\left(k_{i1}x_1+\mathrm{L}\ +k_{iN}x_N\right)=f_i \tag{5}$$

$$\ddot{x}_i=\frac{f_i}{m_{ii}}-\frac{m_{i1}\ddot{x}_1+\mathrm{L}\ +m_{i,i-1}\ddot{x}_{i-1}+m_{i,i+1}\ddot{x}_{i+1}\mathrm{L}\ +m_{iN}\ddot{x}_N}{m_{ii}} - \frac{c_{i1}\dot{x}_1+c_{i2}\dot{x}_2+\mathrm{L}\ +c_{iN}\dot{x}_N}{m_{ii}}-\frac{k_{i1}x_1+k_{i2}x_2+\mathrm{L}\ +k_{iN}x_N}{m_{ii}} \tag{6}$$

$$\ddot{x}_i=\frac{f_i}{m_{ii}}-\frac{k_{i1}x_1+k_{i2}x_2+\mathrm{L}\ +k_{iN}x_N}{m_{ii}} \tag{7}$$

$$\ddot{\ddot{x}}_i=\frac{\dot{f}_i}{m_{ii}}-\frac{k_{i1}\dot{x}_1+k_{i2}\dot{x}_2\mathrm{L}\ +k_{iN}\dot{x}_N}{m_{ii}} \tag{8}$$

$$\frac{\frac{\ddot{x}_i(t+2\Delta t)-\ddot{x}_i(t+\Delta t)}{\Delta t}-\frac{\ddot{x}_i(t+\Delta t)-\ddot{x}_i(t)}{\Delta t}}{\Delta t}=\frac{\dot{f}_i}{m_{ii}}-\frac{k_{i1}\dot{x}_1(t)+k_{i2}\dot{x}_2(t)+\mathrm{L}\ +k_{iN}\dot{x}_N(t)}{m_{ii}} \tag{9}$$

In Eq. (9), we can see that $\ddot{x}_i(t)$ appears on both sides, which may lead to trivial solutions to the parameters of the ARMAX models. To resolve this problem, we define $\ddot{x}_i(t+\Delta t)-\ddot{x}_i(t)$ as a new sequence $y_i(t)$. The final form of the equation is given as Eq. (10), where we can see the relation between signals in different sensors reflects a function of the system's intrinsic properties (*m* and *k*). It is therefore expected that any change in mass and stiffness will be exposed by the change in the coefficients of the ARMAX model if a proper DF is chosen based on the model coefficients.

$$\frac{y_i(t+\Delta t)-y_i(t)}{\Delta t^2}=\frac{\dot{f}_i}{m_{ii}}-\frac{k_{i1}\dot{x}_1(t)+k_{i2}\dot{x}_2(t)+\mathrm{L}\ +k_{iN}\dot{x}_N(t)}{m_{ii}} \tag{10}$$

Comparing Eq. (10) to the ARMAX model in Eq. (1), $y_i(t)$ and $\ddot{x}_1(t)$ are considered as output and input terms, respectively. The errors introduced by ignoring the damping terms and the second derivative of the excitation force can be incorporated into the error terms if we assume they are normally distributed. Therefore, the orders n_a and n_b for the ARMAX model can be chosen as 1 and 1 by comparing the corresponding output and input terms. According to the investigation, n_c is taken as 3 in order to incorporate the influence of errors caused by random ambience force, noise, and by ignoring damping terms. Finally, the ARMAX model for the i^{th} DOF can be expressed as in Eq. (11),

$$y_i(t+\Delta t)+a^i y_i(t)=b_1^i\ddot{x}_1(t)+b_2^i\ddot{x}_2(t)+\mathrm{L}\ +b_N^i\ddot{x}_N(t)+e(t)+d_1e(t-\Delta t)+d_2e(t-\Delta t) \qquad (11)$$

The ARMAX model above is for the i^{th} row in the equation of motion. Therefore, N different ARMAX models can be established for the whole system. Since stiffness and mass matrices are both sparse matrices, the signal of a sensor is expected to be only related to the signals in its adjacent sensors. The ARMAX models can therefore be simplified further, such that only the reference channel and its adjacent channels are included in each ARMAX model. In this respect, we define the sensors adopted by one ARMAX model as a sensor cluster, and the corresponding sensor for output as the reference channel for this sensor cluster.

Building two sets of ARMAX models for the baseline and damaged (or unknown state) structures using the process described above, damage can be identified, located, and quantified by extracting proper DFs from the model coefficients. In the proposed approach, the DF is taken as the

relative difference of $B(q)$ coefficients of damaged and baseline structures. The form of the DF is shown in Eq. (12).

$$DF_{ij} = \frac{b^i_{j,baseline} - b^i_{j,damaged}}{b^i_{j,baseline}} \times 100\%, i \in sensor\ clusters,\ j \in adjacent\ sensors \tag{12}$$

In the next two sections, two case studies are presented where the proposed method is applied to two different numerical models. It is shown that damage can be accurately identified, located, and quantified using output-only acceleration data.

3 *Case Study I: 4-DOF Mass Spring System*

In Case Study I, a 4-DOF mass-spring system (Figure 1) similar to the one used in previous studies (Gül and Catbas 2011; Mei and Gül 2013) is used in this paper. The properties of this system are defined as $m_1 = 3500kg$, $m_2 = m_3 = 2500kg$, $m_4 = 2000kg$, $k_1 = 2 \times 10^7 N/m$ and $k_2 = k_3 = k_4 = k_5 = 7 \times 10^7 N/m$. The stiffness and mass matrices of this system can easily be expressed as in Eq. (13) and Eq. (14).

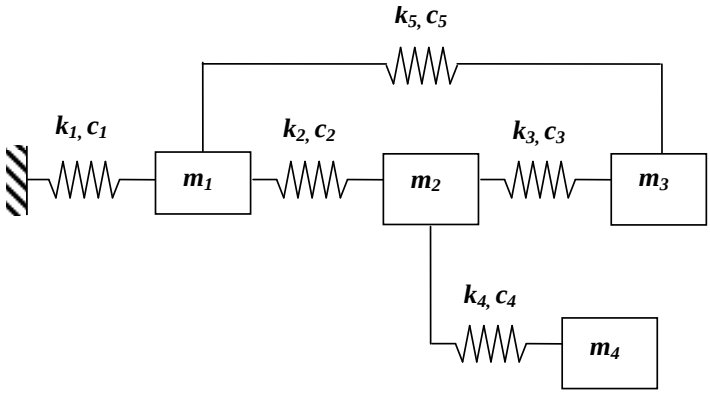

Figure 1. Numerical 4-DOF mass spring model for verification

$$K=\begin{bmatrix} K_{11} & K_{12} & K_{13} & K_{14} \\ K_{21} & K_{22} & K_{23} & K_{24} \\ K_{31} & K_{32} & K_{33} & K_{34} \\ K_{41} & K_{42} & K_{43} & K_{44} \end{bmatrix}=\begin{bmatrix} k_1+k_2+k_5 & -k_2 & -k_5 & 0 \\ -k_2 & k_2+k_3+k_4 & -k_3 & -k_4 \\ -k_5 & -k_3 & k_3+k_5 & 0 \\ 0 & -k_4 & 0 & k_4 \end{bmatrix}$$
$$=\begin{bmatrix} 160 & -70 & -70 & 0 \\ -70 & 210 & -70 & -70 \\ -70 & -70 & 140 & 0 \\ 0 & -70 & 0 & 70 \end{bmatrix} MN/m \tag{13}$$

$$M=\begin{bmatrix} M_{11} & M_{12} & M_{13} & M_{14} \\ M_{21} & M_{22} & M_{23} & M_{24} \\ M_{31} & M_{32} & M_{33} & M_{34} \\ M_{41} & M_{42} & M_{43} & M_{44} \end{bmatrix}=\begin{bmatrix} m_1 & 0 & 0 & 0 \\ 0 & m_2 & 0 & 0 \\ 0 & 0 & m_3 & 0 \\ 0 & 0 & 0 & m_4 \end{bmatrix}=\begin{bmatrix} 3500 & 0 & 0 & 0 \\ 0 & 2500 & 0 & 0 \\ 0 & 0 & 2500 & 0 \\ 0 & 0 & 0 & 2500 \end{bmatrix} kg \tag{14}$$

The classic Rayleigh damping matrix is constructed assuming the damping ratio is 3% for the first two modes. The coefficients a_0=0.72 and a_1=0.0011 are solved from the first and second natural frequencies of the system.

$$C_{ij}=a_0M_{ij}+a_1K_{ij} \tag{15}$$

For this system, five damage patterns are simulated, including stiffness, mass, and damping reduction, as follows:

1) 20% reduction in stiffness k_2;

2) 20% reduction in stiffness k_2 and 10% reduction in stiffness k_4;

3) 20% reduction in mass m_4;

4) 20% reduction in stiffness k_2 and 20% reduction in mass m_2

5) 20% reduction in damping C_{33};

6) Combination of damage patterns 1, 3, and 5.

The excitations are generated as white noise acting on all the DOFs simultaneously in order to simulate the ambient vibration. In order to make the simulations more realistic, 10% noise is added to the signals at all DOFs.

According to the ARMAX-based approach described above, four sensor clusters with different reference channels are created for this system. The first sensor cluster is created with the first DOF as the reference channel, and it includes the first, second, and third DOFs as the adjacent DOFs. For the second sensor cluster, the second DOF is considered as the reference channel and all the DOFs are included as the adjacent channels since this DOF is connected to all the DOFs. The third sensor cluster consists of the first, second, and third DOFs and the reference channel is the third DOF. The last sensor cluster only contains the second and fourth DOFs and the reference channel is the fourth one. Creating the ARMAX models for these four sensor clusters using the data from baseline and damaged structures, the DFs defined in Eq. (12) are extracted.

3.1 *Damage Pattern 1:* $\hat{k}_2 = 0.8 \times k_2$

The first damage pattern simulates a reduction of 20% for stiffness k_2 between the first and second blocks. Table 1 is obtained by applying the DFs mentioned above. Each row of Table 1 represents a sensor cluster, and the four columns of the tables represent the adjacent sensors in the sensor clusters. For instance, the first row is for the first sensor cluster, which has the first DOF as the reference channel. The first sensor cluster includes the first, second, and third DOFs which are connected to it, so the fourth column of the first row is not applicable (N/A). For convenience, the

DFs can each be indexed by their location in the table. For example, the DF in the first row and second column is defined as DF_{12}. It is observed in this table that the DFs for the third and fourth DOFs are close to zero, indicating that the damage is far from these DOFs. The non-zero DFs in the top-left corner show that the damage is related to DOF 1 and DOF 2. The magnitudes represent the contribution of the stiffness reduction. It can be seen in Table 1 that the DF_{21} is -18.88% and DF_{12} is -18.87%, both of which are very close to -20%, which is the applied damage. This indicates the extent of the stiffness reduction in k_2, which is between the first and second DOFs. The -8.90% and -6.61% changes for DF_{11} and DF_{22}, respectively, are caused by the fact that a 20% decrease in k_2 introduces an 8.75% decrease in the total stiffness associated with the first DOF ($0.2k_2/K_{11}$ = $0.2\times7\times10^7/(160\times10^6)$ = 8.75%), and creates a 6.67% decrease in the total stiffness associated with the second DOF ($0.2k_2/K_{22}$ = $0.2\times7\times10^7/(210\times10^6)$ = 6.67%). Especially considering the 10% artificial noise added to the data, these results are deemed very successful in locating and quantifying the damage.

Table 1. Damage features (%) for DP1 in the mass spring system

Reference Channel	1st	2nd	3rd	4th
1st	-8.90	-18.87	-0.91	N/A
2nd	-18.88	-6.61	-0.18	0.33
3rd	-0.17	0.08	-0.06	N/A
4th	N/A	-0.13	N/A	-0.27

3.2 *Damage Pattern 2:* $\hat{k}_2 = 0.8 \times k_2$, $\hat{k}_4 = 0.9 \times k_4$

Damage pattern 2 is obtained as damage pattern 1 plus the reduction of 10% to the element stiffness k_4. From Figure 1, we can see that k_2 is related to DOFs 1 and 2, and k_4 is related to DOFs 2 and 4. In Table 2, it is observed that DF_{11}, DF_{12}, DF_{21} are almost the same as those in Table 1, which again locate and quantify the damage caused by the reduction of k_2. Similarly, the DF_{24}, DF_{42}, DF_{44} between DOFs 2 and 4 with magnitudes of around 10% also represent the influence of the reduction of k_4. The effect of the reduction of k_2 and k_4 on the diagonal stiffness for DOF 2 is $(0.2k_2+0.1k_4)/K_{22} = (0.2+0.1) \times 7\times10^7/(210\times10^6) = 10.00\%$, which is exactly reflected by the value of DF_{22}. It should be emphasized that the reduction of 10.56% for DOF 4 is consistent with the 10% reduction in k_4 since this is the only spring connected to DOF 4. Theoretically, Table 2 should be symmetrical since the stiffnes matrix is symmetrical. The slight asymmetry is mainly caused by the introduced artificial noise. Finally, it is also noted that the 2.33% reduction in DF_{23} can be considering as a false positive. For such cases, determining a threshold based on statistical analysis of DFs obtained from multiple data sets could be very useful (Gül and Catbas 2009). Such a study is not in the scope of this article.

Table 2. Damage features (%) for DP2 in the mass spring system

Reference Channel	1st	2nd	3rd	4th
1st	-8.10	-19.73	0.88	N/A
2nd	-18.22	-10.42	-2.33	-8.62
3rd	0.10	0.45	-0.85	N/A
4th	N/A	-10.67	N/A	-10.56

3.3 *Damage Pattern 3:* $\hat{m}_4 = 0.8 \times m_4$

In the third damage pattern, instead of stiffness reduction, the mass of the fourth DOF has a reduction of 20%. It can be seen from Table 3 that this reduction results in the increase for DF_{42} and DF_{44} around 23-24%, which are both in the fourth sensor cluster. These DFs are explained in Eq. (10), where the mass term is in the denominator and the reduction of this mass by 20% will increase the parameters of the entire sensor cluster by 1/(1-0.2) = 25%. It should be noted that the DFs for the change of mass are asymmetrical, with a very different layout than that for the change of stiffness. This phenomenon is considered as a main characteristic to distinguish between the change of mass and stiffness.

Table 3. Damage features (%) for DP3 in the mass spring system

Reference Channel	1st	2nd	3rd	4th
1st	0.02	-0.82	-0.79	N/A
2nd	0.31	0.24	-0.41	-0.26
3rd	-0.70	-0.09	0.38	N/A
4th	N/A	22.63	N/A	23.91

3.4 *Damage Pattern 4:* $\hat{k}_2 = 0.8 \times k_2$, $\hat{m}_2 = 0.8 \times m_2$

Damage Pattern 4 demonstrates that the damage caused by stiffness and mass change at the same location. As shown in Table 4, the active DFs concentrate on the first and second sensor clusters. In the first row of Table 4, DF_{11} and DF_{12} are close to the corresponding ones in Table 1, which reveal the change of stiffness occurs for DOF 2. The second row shows two features due to the combination of two kinds of damage. DF_{23} and DF_{24} present the pattern mainly introduced by

the mass change without the influence of the stiffness change. DF_{21} and DF_{22} are as a result of the superposition of these two types of damage. In practice, the asymmetry of the DFs is considered as the first step to identify the change of mass, and then specific analysis can be conducted to determine which combination occurs.

Table 4. Damage features (%) for DP4 in the mass spring system

Reference Channel	1st	2nd	3rd	4th
1st	-8.89	-19.52	-0.55	N/A
2nd	2.91	16.59	24.18	24.96
3rd	0.56	-0.86	-0.48	N/A
4th	N/A	0.36	N/A	0.02

3.5 *Damage Pattern 5:* $\hat{C}_{33} = 0.8 \times C_{33}$

In previous damage patterns, the damping matrix has been kept the same even when the mass and stiffness parameters are changed. In this damage pattern, one element of the matrix, C_{33}, is reduced. Although our approach does not seek to identify the change of damping, we would still aim to determine whether or not the damping change will disturb the detection of other changes such as stiffness and mass. In Table 5, it is demonstrated that all the damage features are very close to zero, such that the 20% reduction of C_{33} does not contribute to the DFs. It is therefore expected that the changes of other properties can be identified separately, even if they may lead to a change of damping.

Table 5. Damage features (%) for DP4 in the mass spring system

Reference Channel	1st	2nd	3rd	4th
1st	-0.13	0.81	0.60	N/A
2nd	0.86	-0.31	0.98	0.40
3rd	0.23	0.96	-0.21	N/A
4th	N/A	1.28	N/A	0.04

3.6 *Damage Pattern 6:* $\hat{k}_2 = 0.8 \times k_2$, $\hat{C}_{33} = 0.8 \times C_{33}$ *and* $\hat{m}_4 = 0.8 \times m_4$

To verify the ability to detect various damages at different locations simultaneously, the last damage pattern is introduced, which is a combination of damage patterns 1, 3, and 5. The DFs for this damage pattern are shown in Table 6. In the top-left corner, the DF_{11}, DF_{12}, DF_{21}, and DF_{22} are similar to the corresponding values shown in Table 1, which indicates that the reduction of stiffness has been detected, located, and quantified. For the fourth row, DF_{42} and DF_{44} represent the reduction of mass in the system. It can also be seen that the change of damping has no influence on the DFs.

Table 6. Damage features (%) for DP5 in the mass spring system

Reference Channel	1st	2nd	3rd	4th
1st	-8.57	-18.52	-0.08	N/A
2nd	-17.67	-6.35	-0.06	0.84
3rd	-0.28	0.68	-0.10	N/A
4th	N/A	24.19	N/A	23.87

4 *Case Study II: Application to the IASC-ASCE Benchmark problem*

In order to accelerate the development of SHM methods, some typical benchmark problems that define the realistic conditions and allow researchers to compare the performance of their

respective approaches are necessary. In consideration of this, a task group supported by the International Association of Structural Control (IASC) and the Dynamics Committee of the American Society of Civil Engineers (ASCE) was formed in 1999 (Bernal and Beck 2004; Johnson et al. 2004). The structure selected by this group for investigation was a 4-storey shear type steel frame located at the Earthquake Engineering Research Laboratory of the University of British Columbia (Black and Ventura 1998). As shown in Figure 2, the structure is 2-bays by 2-bays and 3.6 m tall, with a 2.5 m × 2.5 m base.

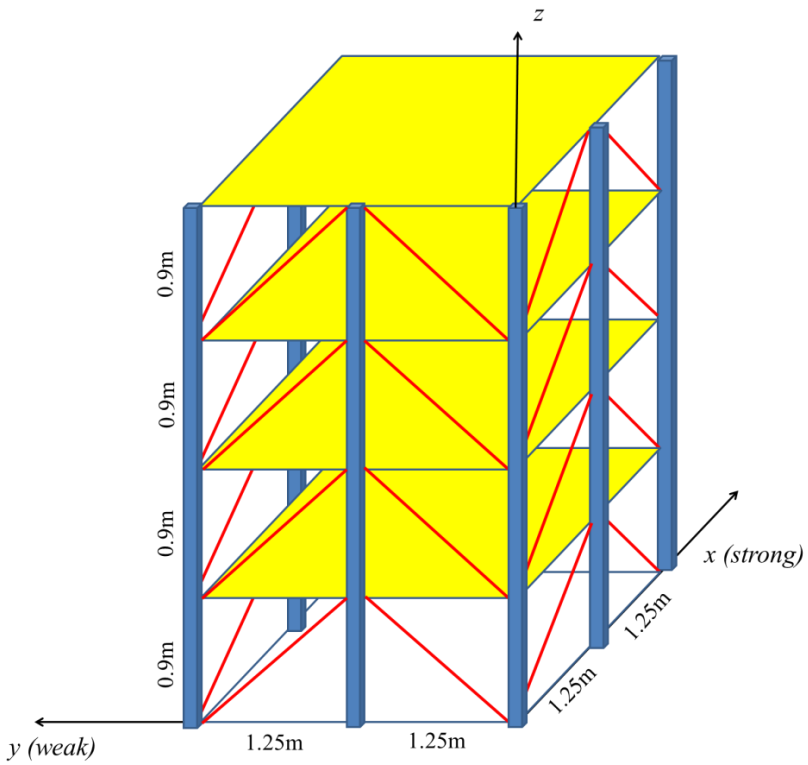

Figure 2. Illustration of the ASCE Benchmark Structure (adapted from Johnson et al. 2004)

A number of research groups have made efforts to apply various approaches to this benchmark problem, either numerically or experimentally. Caicedo et al. (2004) developed an

approach combining natural excitation technique, eigensystem realization algorithm, and least squares method to estimate the stiffness of the ASCE benchmark structure using simulated data. With mass and acceleration information, the approach can correctly detect the location and extent of the damage. Nair et al. (2006) used the Auto-Regressive Moving Average (ARMA) model to fit either analytical or experimental vibration signals of the ASCE benchmark structure, and extracted the DF as a function of the first three auto-regressive components. In addition to the existence of damage, they also introduced localization indices to identify the location of the damage. Lynch (2005) used experimental data of the ASCE benchmark structure excited by a shaker to estimate transfer function poles using traditional system identification methods. By comparing the location of poles for an unknown state to those of the baseline state, the damage can be accurately identified. However, excitation data, which is very difficult to obtain in realistic structures, is used in this approach. Despite these successful attempts, some challenges are still not addressed. Thus, our new approach aims to detect, locate, and quantify the damage caused by mass and stiffness changes separately using output data only.

As the second case study, the proposed approach is tested under simulated data in phase I of the IASC-ASCE benchmark problem using the 120 DOF finite element model. For this model, the excitations are modeled as independent filtered Gaussian white noises, and are applied one per floor at the center of each floor as approximating wind or other ambient excitations. The excitations can be added either in strong (x) direction or weak (y) direction. Considering that the properties of this shear-type structure in one direction are mainly related to the vibrations in the

corresponding direction, two directions of excitation are applied separately in order to detect the damage in different directions. There are four accelerometers on each floor, two of which are to monitor the accelerations in the *x* direction, and the other two of which are for the *y* direction (Figure 3). To simulate the errors caused by the measurement or environment, 10% noise is imposed to all the acceleration signals in the sensors. Figure 4 demonstrates the acceleration signals of the baseline structure acquired by the sensors located as a_{x1} in Figure 3. In order to obtain the translational acceleration of the floor and reduce the effect of noise, the average is taken of the two sensors in the same direction.

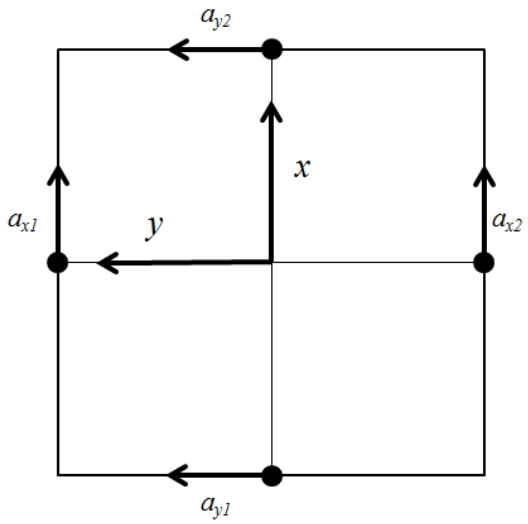

Figure 3. Placements and directions of sensors and excitations

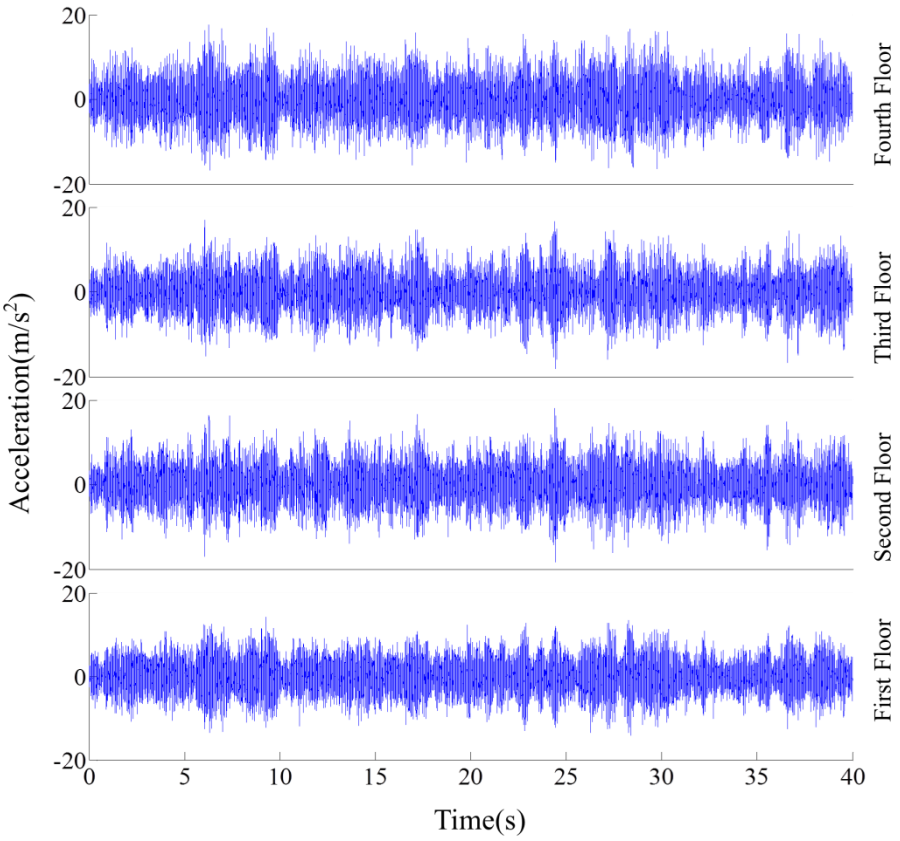

Figure 4. Acceleration data for each floor with 10% artificial noise

There are six damage patterns defined in the benchmark problem to simulate major damage, minor damage, asymmetrical damage, etc. (Johnson et al 2004). These damage patterns are introduced by removing different braces, and mainly manifest as stiffness reduction. In addition, two damage patterns simulating the mass reduction, referred to as Damage Patterns M1 and M2, are also demonstrated in this paper. The eight damage patterns included in this paper are outlined below:

• Damage Pattern 1 (DP1): Removal of all braces on the first floor;

• Damage Pattern 2 (DP2): Removal of all braces on the first and third floors;

• Damage Pattern 3 (DP3): Removal of one brace on the first floor;

• Damage Pattern 4 (DP4): Removal of one brace on one side of the first and third floors;

• Damage Pattern 5 (DP5): Damage Pattern 4 + unscrewing of the left end of the north floor beam at the first floor on the west face of the structure;

• Damage Pattern 6 (DP6): Reduction of the stiffness of a brace to two-thirds of its original value;

• Damage Pattern M1 (DPM1): Reduction of mass on the fourth floor; and

• Damage Pattern M2 (DPM2): Damage Pattern M1 + Damage Pattern 1.

Note that the last two damage patterns were not included in the original benchmark damage cases; rather, they were created for this study to demonstrate the capability of the method for detection of changes in mass.

4.1 *Damage Pattern 1: All braces of the first floor are broken*

The first damage pattern shows a stiffness reduction of the first floor due to the removal of all the braces on the first floor. As described above, the vibration in the *x* direction can be used to detect the change of properties in the *x* direction (strong direction), and the vibration in the *y* direction is for damage detection in the *y* direction (weak direction). The DFs calculated using the proposed method are shown in Table 7 for the *x* and *y* directions, respectively. As has already been discussed in section 3 of this paper, each row in these tables represents a sensor cluster. For the *x* direction, all valid DFs except $DF_{11,x}$, which has a value of -25.64%, are very close to zero. This shows that the damage is only related to the change of properties on the first floor. Considering that the original

stiffness for the first floor in the *x* direction is 2.1320 $\times 10^8$ N/m, and that the damaged stiffness is 1.6497 $\times 10^8$ N/m (Johnson et al. 2004), the reduction of stiffness caused by the elimination of the braces is -(2.1320-1.6497)/2.1320 = -22.60%, which is very close to the DF (-25.64%) shown in the table. This verifies that this approach is able to measure the severity of the damage quite accurately. Similarly, the DFs for the *y* direction demonstrate again that the damage occurred on the first floor. The $DF_{11,y}$ for the *y* direction is -36.34%, which is close to the stiffness reduction in the *y* direction due to the removal of braces (-(1.3581-0.8758)/1.3581 = -35.51%), indicating that the braces have more contribution to stiffness in the *y* direction than in the *x* direction.

Table 7. Damage features (%) for DP1 in the IASC-ASCE benchmark problem

Reference Channel		1st	2nd	3rd	4th
x direction	1st	-25.64	-1.29	N/A	N/A
	2nd	0.22	-0.72	0.68	N/A
	3rd	N/A	-1.13	-1.13	-1.34
	4th	N/A	N/A	-1.11	0.01
y direction	1st	-36.34	0.47	N/A	N/A
	2nd	1.61	0.03	0.02	N/A
	3rd	N/A	0.56	0.36	0.25
	4th	N/A	N/A	-0.50	0.91

4.2 *Damage Pattern 2: All braces of first and third floor are broken*

Damage pattern 2 involves the removal of the braces on the first and third floors. It is thus expected that the damage features related to the first and third floors will be non-zero values. It is observed from Table 8 that the $DF_{11,x}$ for the first row and first column is -24.89%, which is almost the same as the corresponding value in Table 7, indicating that the damage for the first floor can still be located and quantified. It can also be seen that for *x* direction the four DFs between the second and third sensors reflect how the removal of the braces on the third floor influences the stiffness. The magnitudes, meanwhile, imply that the removal of the braces results in reductions of 26.35% and 29.19% in total stiffness of the second and third floors, respectively.

Table 8. Damage features (%) for DP2 in the IASC-ASCE benchmark problem

Reference Channel		1st	2nd	3rd	4th
x direction	1st	-24.89	3.97	N/A	N/A
	2nd	-0.10	-26.35	-50.05	N/A
	3rd	N/A	-51.74	-29.19	-3.53
	4th	N/A	N/A	1.93	0.36
y direction	1st	-36.26	0.09	N/A	N/A
	2nd	0.74	-36.86	-72.61	N/A
	3rd	N/A	-73.30	-39.46	-3.85
	4th	N/A	N/A	-0.40	0.27

This damage also creates an approximately 50% reduction in the stiffness between the second and third floors. For the *y* direction, the patterns of DFs are similar, but the absolute values are larger, which means that the braces make more contribution to the stiffness in the *y* direction. It should also

be mentioned that other DFs are not exactly zero, mostly due to the 10% noise added to the data. However, since these values are significantly smaller than the other DFs where the damage is observed, the damage is not hidden by the false-positive results. For real implementation, different statistical analyses can be conducted to define a threshold value in order to minimize such false positives and negatives (Gül and Catbas 2009).

4.3 *Damage Pattern 3: One brace of first floor is broken*

Damage pattern 3 is minor compared to damage patterns 1 and 2. In damage pattern 3, only one brace of the first floor in the *y* direction is removed, which would lead to a smaller stiffness reduction in the structure. In Table 9, it is observed that all the DFs for the *x* direction are very close to zero. This is to be expected since the removed brace would have only provided stiffness in the *y* direction, such that its removal will not influence the stiffness in the *x* direction. For the *y* direction, it can be seen that the patterns of DFs are similar to corresponding ones in Table 7, since the removal of the brace only influences the stiffness for the first floor. The $DF_{11,y}$ is -10.52% which is around 1/4 of the corresponding DF in Table 7. Given that there are four braces in each direction on each floor, it is reasonable that removal of one brace should lead to 1/4 stiffness reduction compared to the case where all of the braces were removed.

Table 9. Damage features (%) for DP3 in the IASC-ASCE benchmark problem

Reference Channel		1st	2nd	3rd	4th
x direction	1st	0.73	0.02	N/A	N/A
	2nd	-1.07	1.02	1.17	N/A
	3rd	N/A	1.18	0.22	-0.69
	4th	N/A	N/A	1.99	2.41
y direction	1st	-10.52	-0.29	N/A	N/A
	2nd	0.73	0.37	0.97	N/A
	3rd	N/A	0.35	-0.10	-0.20
	4th	N/A	N/A	-0.29	-0.43

4.4 *Damage Pattern 4: One brace for each of the first floor and third floor is broken*

Damage pattern 4 involves only minor damage compared to damage pattern 2. Only one brace is broken on each of the first (in *y* direction) and third floors (in *x* direction), which introduces an asymmetrical and torsional behavior into the structure. It can be seen in Table 10 that the DFs for the *x* direction related to the second and third floors have large magnitudes, whereas the corresponding DFs for the *y* direction are very close to zero. The reason for this important finding is that the removal of the brace on the third floor is only in the *x* direction, so it will not affect the DFs in the *y* direction. Also note that the DFs in the *x* direction for the second and third floors are around 1/4 of those in Table 8, for the same reason described with respect to damage pattern 3. Furthermore, for the *y* direction it shows the same DFs as those in Table 9. It is therefore observed that the proposed approach can locate and quantify damage in different directions separately, even if the structure is asymmetrical.

Table 10. Damage features (%) for DP4 in the IASC-ASCE benchmark problem

Reference Channel		1st	2nd	3rd	4th
x direction	1st	-0.03	2.04	N/A	N/A
	2nd	2.32	-8.06	-15.71	N/A
	3rd	N/A	-15.59	-7.57	1.69
	4th	N/A	N/A	-0.91	-1.69
y direction	1st	-10.28	0.32	N/A	N/A
	2nd	1.64	0.59	-0.12	N/A
	3rd	N/A	-0.35	-0.10	-0.20
	4th	N/A	N/A	0.29	0.43

4.5 *Damage Pattern 5: Damage Pattern 4 + unscrewing of the left end of the north floor beam at the first floor on the west face of the structure*

Damage pattern 5 is very close to damage pattern 4. In addition to the brace removals in damage pattern 4, only one beam is unscrewed on the first floor. From Table 11 it can be observed that the DFs are almost the same as those in Table 10, which indicates that the damage pattern 4 is detected and the damage introduced by the unscrewing of the beam is hidden. According to Johnson et al. (2004), it is observed that the difference between the stiffness matrices for damage patterns 4 and 5 is quite small. We thus conclude that the reason the unscrewing of the beam cannot be detected is that the damage is not noticeably reflected in the change in stiffness of the finite element model.

Table 11. Damage features (%) for DP5 in the IASC-ASCE benchmark problem

Reference Channel		1st	2nd	3rd	4th
x direction	1st	-0.26	1.18	N/A	N/A
	2nd	0.32	-6.92	-13.44	N/A
	3rd	N/A	-14.41	-8.49	-0.77
	4th	N/A	N/A	-0.47	0.16
y direction	1st	-10.20	-0.24	N/A	N/A
	2nd	1.18	-0.53	-0.77	N/A
	3rd	N/A	0.67	0.42	0.61
	4th	N/A	N/A	0.46	0.43

4.6 *Damage Pattern 6: Area of one brace on one side of the first storey is reduced to 2/3*

Damage pattern 6 is very close to damage pattern 1, which involves stiffness reduction for the first floor. However, damage pattern 6 is even smaller than pattern 1, since no braces are removed but instead the stiffness of one brace on the first floor is reduced to 2/3 of its original value. Similarly, it can be seen in Table 12 that the DFs for the *x* direction are very small, which means that the damage is not in the *x* direction. However, it is also noted that $DF_{12,x}$ and $DF_{21,x}$ are both greater than 2% (because of the 10% artificial noise added to the data), which may cause them to be confused with the minor real damage applied in the *y* direction. For the *y* direction, a -4.01% reduction in $DF_{11,y}$ is identified, which demonstrates the slight stiffness reduction on the first floor. The magnitude of -4.01% here is approximately 1/3 of the -10.52% magnitude in Table 9, which exactly reflects the severity of the damage (1/3 stiffness reduction in the brace). Note that all of the other DFs in this table are close to zero.

Table 12. Damage features (%) for DP6 in the IASC-ASCE benchmark problem

Reference Channel		1st	2nd	3rd	4th
x direction	1st	0.81	2.04	N/A	N/A
	2nd	2.84	0.62	0.22	N/A
	3rd	N/A	0.16	0.76	1.28
	4th	N/A	N/A	1.35	0.74
y direction	1st	-4.01	-0.63	N/A	N/A
	2nd	0.92	0.02	0.06	N/A
	3rd	N/A	-0.49	0.34	0.60
	4th	N/A	N/A	-0.10	0.18

4.7 *Damage Pattern M1: Mass of fourth floor is reduced by 20%*

From the results for damage patterns 1-6, it is demonstrated that the change of stiffness can be very accurately detected, located, and quantified using the proposed approach. In this section, a reduction of 20% to the mass on the fourth floor is introduced to test the capability of the methodology for identification of mass changes. It can be seen in Table 13 that the DFs for the fourth sensor cluster for both *x* and *y* directions are very large (around 25%) while the other values are very close to zero. As before, the magnitude of 25% in the DFs for 20% reduction in the mass can be deduced from Eq. 10, where the mass term is in the denominator. It should be noted that the DFs for the change of mass are asymmetrical, just as shown for the mass spring system, and same in both *x* and *y* directions, which can be considered as the main differences between change of mass and change of stiffness.

Table 13. Damage features (%) for DPM1 in the IASC-ASCE benchmark problem

Reference Channel		1st	2nd	3rd	4th
x direction	1st	-0.15	1.46	N/A	N/A
	2nd	1.82	-0.18	-0.49	N/A
	3rd	N/A	-0.62	-0.15	0.40
	4th	N/A	N/A	24.84	24.48
y direction	1st	-0.78	0.26	N/A	N/A
	2nd	0.08	-0.78	-1.28	N/A
	3rd	N/A	-0.65	-0.66	-0.71
	4th	N/A	N/A	25.34	25.05

4.8 *Damage Pattern M2: Damage Pattern 1 + Damage Pattern M1*

From previous sections, the capability of this approach to identify and quantify change of mass and change of stiffness, respectively, has been verified. Now damage consisting of changes of both mass and stiffness is introduced by combining damage pattern 1 and damage pattern M1. The DFs for this damage pattern are demonstrated in Table 14. The $DF_{11,x}$ and $DF_{11,y}$ related to the first floor are close to the corresponding DFs in Table 7, indicating that a change of stiffness is detected. Similarly, The $DF_{43,x}$, $DF_{44,x}$, $DF_{43,y}$ and $DF_{44,y}$, which demonstrate the change of mass, are the same as those in Table 13. It is noted that a change of mass and stiffness can be distinguished by the characteristic that the DFs for mass change are not symmetrical, i.e., that change affects only rows in the table. It is therefore concluded that the proposed approach is able to accurately identify, locate, and quantify damage, and to distinguish change of mass and change of stiffness separately, even when they occur simultaneously. Having said this, it is acknowledged that noticing these symmetrical and

asymmetrical changes in real-life data may not be as easy but these findings are still very valuable for separating the stiffness and mass changes using output-only data in SHM applications.

Table 14. Damage features (%) for DPM2 in the IASC-ASCE benchmark problem

Reference Channel		1st	2nd	3rd	4th
x direction	1st	-24.03	2.56	N/A	N/A
	2nd	2.54	0.11	0.72	N/A
	3rd	N/A	-0.73	-0.21	0.26
	4th	N/A	N/A	24.78	25.31
y direction	1st	-36.03	0.39	N/A	N/A
	2nd	-0.53	-1.38	1.05	N/A
	3rd	N/A	0.18	0.04	-1.23
	4th	N/A	N/A	24.56	25.58

5 *Conclusions*

In this study, a novel approach based on time series modeling has been presented for damage detection. In this approach, ARMAX models adopting output-only data have been created for different sensor clusters. In this way, an anomaly can be identified by considering the damage features extracted from the difference between coefficients of ARMAX models for baseline and damaged structures. The approach has been applied to a 4-DOF mass spring system and then to phase I of the shear type IASC-ASCE benchmark problem. The results show that change of stiffness and change of mass can be detected and located separately. In addition, the magnitude of the change can be accurately reflected by the DF values. This constitutes the first approach of its

kind which can distinguish between change of stiffness and change of mass in order to accurately measure the severity of an anomaly. On a theoretical level, this approach achieves level 3 damage detection as defined by Rytter (1993). As a potential direction for future study, the authors acknowledge that experimental research should be carried out to test the suitability of this theoretical approach for real-life structures.

References

Beck, J., and Bernal, D. (2001). "A Benchmark Problem for Structural Health Monitoring." *Experimental Techniques*, 25(3), 49-52.

Bernal, D., and Beck, J. (2004). "Preface to the Special Issue on Phase I of the IASC-ASCE Structural Health Monitoring Benchmark." *Journal of Engineering Mechanics, ASCE*, 130(1), 1–2.

Black, C. J., and Ventura, C. E. (1998). "Blind Test on Damage Detection of a Steel Frame Structure." *Proceedings of the 16th International Modal Analysis Conference (IMAC XVI)*, Santa Barbara, CA , 1, 623-629.

Box, G. E., Jenkins, G. M., and Reinsel, G. C. (2013). "Time Series analysis: Forecasting and Control, 4th Edition." John Wiley & Sons, Hoboken, NJ.

Brockwell, P. J., and Davis, R. A. (2002). "Introduction to Time Series and Forecasting, 2nd Edition", Springer, Berlin, Germany.

Caicedo, J. M., Dyke, S. J., and Johnson, E. A. (2004). "Natural Excitation Technique and Eigensystem Realization Algorithm for Phase I of the IASC-ASCE Benchmark Problem: Simulated Data." *Journal of Engineering Mechanics, ASCE,* 130(1), 49-60.

Carden, E. P., and Brownjohn, J. M. (2008). "ARMA Modelled Time-series Cl assification for Structural Health Monitoring of Civil Infrastructure." *Mechanical Systems and Signal Processing*, 22(2), 295-314.

Catbas, F. N., Ciloglu, S., Hasancebi, O., Grimmelsman, K., and Aktan, A. (2007). "Limitations in Structural Identification of Large Constructed Structures." *Journal Structural Engineering, ASCE,* 133(8), 1051–1066.

Chang, C. C., Chang, T. Y. P., Xu, Y. G., and Wang, M. L. (2000). "Structural Damage Detection Using an Iterative Neural Network." *Journal of Intelligent Material Systems and Structures*, 11(1), 32-42.

Cheng, L., and Tian, G. Y. (2012). "Comparison of Non-destructive Testing Methods on Detection of Delaminations in Composites." *Journal of Sensors*, 2012, 1-7.

Dharap, P., Koh, B. H., and Nagarajaiah, S. (2006). "Structural Health Monitoring Using ARMarkov Observers." *Journal of Intelligent Material Systems and Structures*, 17(6), 469-481.

Fan, W., and Qiao, P. (2011). "Vibration-based Damage Identification Methods: a Review and Comparative Study." *Structural Health Monitoring*, 10(1), 83-111.

Figueiredo, E., Farinholt, K. M., Lee, J. R., Farrar, C. R., and Park, G. (2012). "Use of time-series predictive models for piezoelectric active-sensing in structural health monitoring applications." *Journal of Vibration and Acoustics*, 134(4), 041014, 10p.

Gül, M., and Catbas, F. N. (2009). "Statistical Pattern Recognition for Structural Health Monitoring using Time Series Modeling: Theory and Experimental Verifications." *Mechanical Systems and Signal Processing*, 23(7), 2192-2204.

Gül, M., and Catbas, F. N. (2011). "Structural Health Monitoring and Damage Assessment Using a Novel Time Series Analysis Methodology with Sensor Clustering." *Journal of Sound and Vibration*, 330(6), 1196-1210.

Han, L. Z., Zhang, J. Q., and Yang, Y. (2014). "Optimal Placement of Sensors for Monitoring Systems on Suspension Bridges using Genetic Algorithms." *Applied Mechanics and Materials*, 530, 320-331.

Hearn, G., and Testa, R. B. (1991). "Modal Analysis for Damage Detection in Structures." *Journal of Structural Engineering, ASCE*, 117(10), 3042-3063.

Hoła, J., and Schabowicz, K. (2010). "State-of-the-art Non-destructive Methods for Diagnostic Testing of Building Structures–Anticipated Development Trends." *Archives of Civil and Mechanical Engineering*, 10(3), 5-18.

Hou, Z., Noori, M., and Amand, R. (2000). "Wavelet-Based Approach for Structural Damage Detection." *Journal of Engineering Mechanics, ASCE*, 126(7), 677–683.

Im, S. B., Hurlebaus, S., and Kang, Y. J. (2011). "Summary Review of GPS Technology for Structural Health Monitoring." *Journal of Structural Engineering, ASCE*, 139(10), 1653-1664.

Inaudi, D., and Glisic, B. (2008). "Overview of 40 Bridge Monitoring Projects using Fiber Optic Sensors." *Conference CD, 4TH International Conference on Bridge Maintenance, Safety and Management (IABMAS '08),* Seoul, Korea.

Jafarkhani, R., and Masri, S. F. (2011). "Finite Element Model Updating using Evolutionary Strategy for Damage Detection." *Computer - Aided Civil and Infrastructure Engineering*, 26(3), 207-224.

Ji, X., Fenves, G. L., Kajiwara, K., and Nakashima, M. (2010). "Seismic Damage Detection of a Full-Scale Shaking Table Test Structure." *Journal of Structural Engineering, ASCE*, 137(1), 14-21.

Johnson, E., Lam, H., Katafygiotis, L., and Beck, J. (2004). "Phase I IASC-ASCE Structural Health Monitoring Benchmark Problem Using Simulated Data." *Journal of Engineering Mechanics, ASCE*, 130(1), 3–15.

Kessler, S. S., Spearing, S. M., and Soutis, C. (2002). "Damage Detection in Composite Materials using Lamb Wave Methods." *Smart Materials and Structures*, 11(2), 269.

Lynch, J. *(2005). "*Damage Characterization of the IASC-ASCE Structural Health Monitoring Benchmark Structure by Transfer Function Pole Migration.*" Proceedings of the ASCE Structures Congress and the Forensic Engineering Symposium*, New York, NY, 845-854.

Lynch, J. P., and Loh, K. J. (2006). “A Summary Review of Wireless Sensors and Sensor Networks for Structural Health Monitoring.” *Shock and Vibration Digest*, 38(2), 91-130.

Levy, H., and Lessman, F., (1992). “Finite Difference Equations." Dover Publications, Mineola, NY.

Mei, Q., and Gül, M. (2013). “An Improved Methodology for Anomaly Detection Based on Time Series Modeling.” *Proceedings of the 31st International Modal Analysis Conference* (*IMAC XXXI*), Garden Grove, CA, 277-281.

Meruane, V., and Heylen, W. (2011). “An Hybrid Real Genetic Algorithm to Detect Structural Damage using Modal Properties.” *Mechanical Systems and Signal Processing*, 25(5), 1559-1573.

Moaveni, B., Conte, J. P., and Hemez, F. M. (2009). “Uncertainty and Sensitivity Analysis of Damage Identification Results Obtained using Finite Element Model Updating.” *Computer‐Aided Civil and Infrastructure Engineering*, 24(5), 320-334.

Moaveni, B., Hurlebaus, S., and Moon, F. (2012). “Special Issue on Real-World Applications of Structural Identification and Health Monitoring Methodologies.” *Journal of Structural Engineering, ASCE,* 139(10), 1637-1638.

Monroig, E., and Fujino, Y., (2006). “Damage Identification Based on a Local Physical Model for Small Cluster of Wireless Sensors.” *the 1st Asia-Pacific Workshop on Structural Health Monitoring*, Yokohama, Japan.

Nair, K. K., Kiremidjian, A. S., and Law, K. H. (2006). "Time Series-Based Damage Detection and Localization Algorithm with Application to the ASCE Benchmark Structure." *Journal of Sound and Vibration,* 291(1), 349-368.

Nigro, M. B., Pakzad, S. N., and Dorvash, S. (2014). "Localized Structural Damage Detection: A Change Point Analysis." Accepted to *Computer‐Aided Civil and Infrastructure Engineering*.

Pandey, A. K., Biswas, M., and Samman, M. M. (1991). "Damage Detection from Changes in Curvature Mode Shapes." *Journal of sound and vibration,* 145(2), 321-332.

Rytter, A. *(1993*). "Vibration Based Inspection of Civil Engineering Structures." PhD dissertation, University of Aalborg, Aalborg, Denmark.

Shiradhonkar, S. R., and Shrikhande, M. (2011). "Seismic Damage Detection in a Building Frame via Finite Element Model Updating." *Computers and Structures,* 89(23), 2425-2438.

Sipple, J. D. and Sanayei, M. (2013). "Finite Element Model Updating Using Frequency Response Functions and Numerical Sensitivities," *Structural Control and Health Monitoring,* 21(5), 784-802.

Sohn, H., Farrar, C. R., Hunter, N. F., and Worden, K. (2001). "Structural Health Monitoring Using Statistical Pattern Recognition Techniques." *Journal of Dynamic Systems, Measurement, and Control*, 123(4), 706-711.

Taha, M. M. R. (2010). "A Neural-wavelet Technique for Damage Identification in the ASCE Benchmark Structure Using Phase II Experimental Data." *Advances in Civil Engineering*, 2010, 1-13.